BEDROCK GEOLOGIC MAP OF THE NORTHERN FAIRBANKS MINING DISTRICT, CIRCLE QUADRANGLE, ALASKA

J.E. Athey, L.K. Freeman, R.J. Newberry, M.B. Werdon, D.J. Szumigala, and R.R. Lessard

Preliminary Interpretive Report 2022-2

2022
STATE OF ALASKA
DEPARTMENT OF NATURAL RESOURCES
DIVISION OF GEOLOGICAL & GEOPHYSICAL SURVEYS

STATE OF ALASKA
Mike Dunleavy, Governor

DEPARTMENT OF NATURAL RESOURCES
Akis Gialopsos, Acting Commissioner

DIVISION OF GEOLOGICAL & GEOPHYSICAL SURVEYS
David L. LePain, State Geologist & Director

Publications produced by the Division of Geological & Geophysical Surveys are available to download from the DGGS website (dggs.alaska.gov). Publications on hard-copy or digital media can be examined or purchased in the Fairbanks office:

Alaska Division of Geological & Geophysical Surveys (DGGS)
3354 College Road | Fairbanks, Alaska 99709-3707
Phone: 907.451.5010 | Fax 907.451.5050
dggspubs@alaska.gov | dggs.alaska.gov

DGGS publications are also available at:

Alaska State Library, Historical
Collections & Talking Book Center
395 Whittier Street
Juneau, Alaska 99801

Alaska Resource Library and
Information Services (ARLIS)
3150 C Street, Suite 100
Anchorage, Alaska 99503

Suggested citation:
Athey, J.E., Freeman, L.K., Newberry, R.J., Werdon, M.B., Szumigala, D.J., and Lessard, R.R., 2022, Bedrock geologic map of the northern Fairbanks mining district, Circle Quadrangle, Alaska: Alaska Division of Geological & Geophysical Surveys Preliminary Interpretive Report 2022-2, 24 p., 1 sheet.
https://doi.org/10.14509/30891

BEDROCK GEOLOGIC MAP OF THE NORTHERN FAIRBANKS MINING DISTRICT, CIRCLE QUADRANGLE, ALASKA

J.E. Athey[1], L.K. Freeman[2], R.J. Newberry[1], M.B. Werdon[1], D.J. Szumigala[1], and R.R. Lessard[3]

INTRODUCTION

This booklet accompanies Preliminary Interpretive Report 2022-2, a 1:50,000-scale bedrock geologic map of the northern Fairbanks mining district, covering parts of the Circle A-4, A-5, B-4, and B-5 quadrangles. The booklet contains unit descriptions and supporting information. The 188-square-mile study area is 55 direct miles northeast of Fairbanks, straddling the Steese Highway between miles 66 and 85. The field area is coincident with the northern tip of the Fairbanks mining district, Alaska's largest historic producer at just less than 17 million troy ounces of gold (Twelker and others, 2022). Faith Creek and its tributaries are intermittently mined for placer gold, and local creeks are popular with recreational placer miners. This area is within the northeast-oriented trend between plutonic-related gold mineralization in the central Fairbanks mining district and placer gold deposits in the northwest Circle mining district. Nearby infrastructure would facilitate mineral development, such as good access from the highway and a few trails, in addition to nearby power from the high-voltage power lines of the Fort Knox gold mine located 25 miles to the southwest.

During June 2007, personnel from the Alaska Division of Geological & Geophysical Surveys (DGGS) and the University of Alaska Fairbanks spent approximately 189 person-days conducting field work in the northeast Fairbanks area. The study area is located within the Yukon-Tanana Uplands, and elevations in the map area range from 1,417 to 4,184 feet. Topography consists of moderate- to steep-sided ridges and domes vegetated with tundra, spruce, aspen, poplar, alder, and willow. About half of the study area was partially burned in the 2004 Boundary wildfire, and exposed bedrock was discovered during 2007 fieldwork in places that were previously heavily vegetated. Natural outcrops commonly occur along hilltops, steep slopes, and in incised stream valleys. The map area covers the central portion of the Northeast Fairbanks airborne geophysical survey (Burns and others, 2006; superseded by Burns and others, 2019a). Total field magnetic and electromagnetic geophysical data aided our bedrock mapping, especially in areas covered by vegetation and unconsolidated Quaternary deposits. For example, our interpretation of the geophysical data reveals subtle differences in the compositions of similar-looking rocks and structures that would otherwise remain undetected by conventional surface mapping methods. New geologic mapping with interpretation of geophysical data will lead to: (1) a better understanding of the lithologic and tectonic framework of Interior Alaska, (2) baseline geologic-materials and -hazards data for future construction of infrastructure and settlements, and the maintenance of current infrastructure, including the Steese Highway, (3) geologic-resource data critical to land-use decisions, and (4) a foundation of geologic knowledge that will encourage mineral exploration investment in the northern section of the Fairbanks mining district.

[1] Alaska Division of Geological & Geophysical Surveys, 3354 College Road, Fairbanks, Alaska 99707
[2] Retired Alaska Division of Geological & Geophysical Surveys, 3354 College Rd, Fairbanks, AK 99709
[3] Alaska Division of Mining, Land and Water, 550 W. 7th Ave, Suite 1360, Anchorage, AK 99501

Geologic units are defined by field observations and analysis of samples collected at more than 2,222 stations. Unit descriptions are also based on the petrographic examination and modal analysis of 301 thin sections (this study), 116 thin sections collected in the Circle Quadrangle by the U.S. Geological Survey from 1979–1981, and 26 thin sections from the 1986 Lime Peak–Mt. Prindle project (Smith and others, 1987). Metamorphic rocks and younger, unmetamorphosed igneous rocks were primarily defined by chemical composition, examination of hand samples, and petrography. Forty-four rock samples were analyzed for major- and minor-oxide by a commercial analytical laboratory (Athey and others, 2008), and trace-elements by the University of Alaska Fairbanks (app. A). These data are used to suggest possible protoliths of metamorphosed and altered rocks, identify types of alteration, and assign trace-element-indicated tectonic settings to igneous and metamafic rocks (app. B). Non-carbonate carbon in 16 samples was measured by a commercial analytical laboratory (app. C). Garnet–biotite geothermometry and garnet–plagioclase–muscovite–biotite equilibria geobarometry were conducted on 16 samples to assess the metamorphic history of the units (app. D). Five $^{40}Ar/^{39}Ar$ ages were used to constrain timing of igneous events, mineralization, and metamorphism in the northeast Fairbanks area (app. E; Layer and others, in prep.). One U-Pb detrital zircon age provides a maximum age of the metamorphosed sedimentary rocks and for regional unit correlations (app. F; O'Sullivan and Athey, in prep.).

To evaluate the mineral-resource potential of the northeast Fairbanks area, 128 samples of visibly mineralized rock, or rocks exhibiting features associated with mineralization, were analyzed for geochemical trace elements (Athey and others, 2008). In addition, 67 stream-sediment samples were collected for geochemical trace-element analysis. The stream-sediment geochemical study was conducted over the proposed Mount Ryan Remote Recreational Cabin Staking Area under consideration by Alaska's Division of Mining, Land & Water (DMLW) in 2007, which coincides with the southeast corner and about 30 percent of the study area. DGGS provided these timely geologic data to DMLW to assist in determining whether this area should be opened to settlement and closed to mineral exploration and development. Knowledge of the area's mineral potential was instrumental in DMLW's decision to relocate a portion of the 2007 proposed Mount Ryan Remote Recreational Cabin Sites Staking Area to an area with lower perceived mineral potential.

LITHOLOGIC DESCRIPTIONS, STUDIES, AND INTERPRETATIONS

Geophysics and Structural Interpretation

The study area covers parts of the Circle A-4, A-5, B-4, and B-5 quadrangles (fig. 1). In terms of geophysical mapping, the area lacks the magnetic and conductive geophysical signatures characteristic of the eclogite-facies Chatanika terrane of the Fairbanks area but does contain the geophysical signatures suggestive of the amphibolite-facies Fairbanks schist and gold-related plutons seen in the Fairbanks area (Newberry and others, 1996; Burns and others, 2006, 2019b). East–northeast-trending geophysical signatures largely continuous from the southwest, corresponding to metamorphic lithologies, are clearly cut by the northeast-trending, near-vertical 'Swamp Saddle fault' in the map area; matching geophysical anomalies suggest approximately 5–10 miles of left-lateral displacement. Contrasting geophysical signatures on the southeast side of the fault indicate a significant change in geology; this area is mapped as quartzite and grit-bearing quartzite (unit €Zq), correlative with similar Interior Alaska rocks to the north and west of

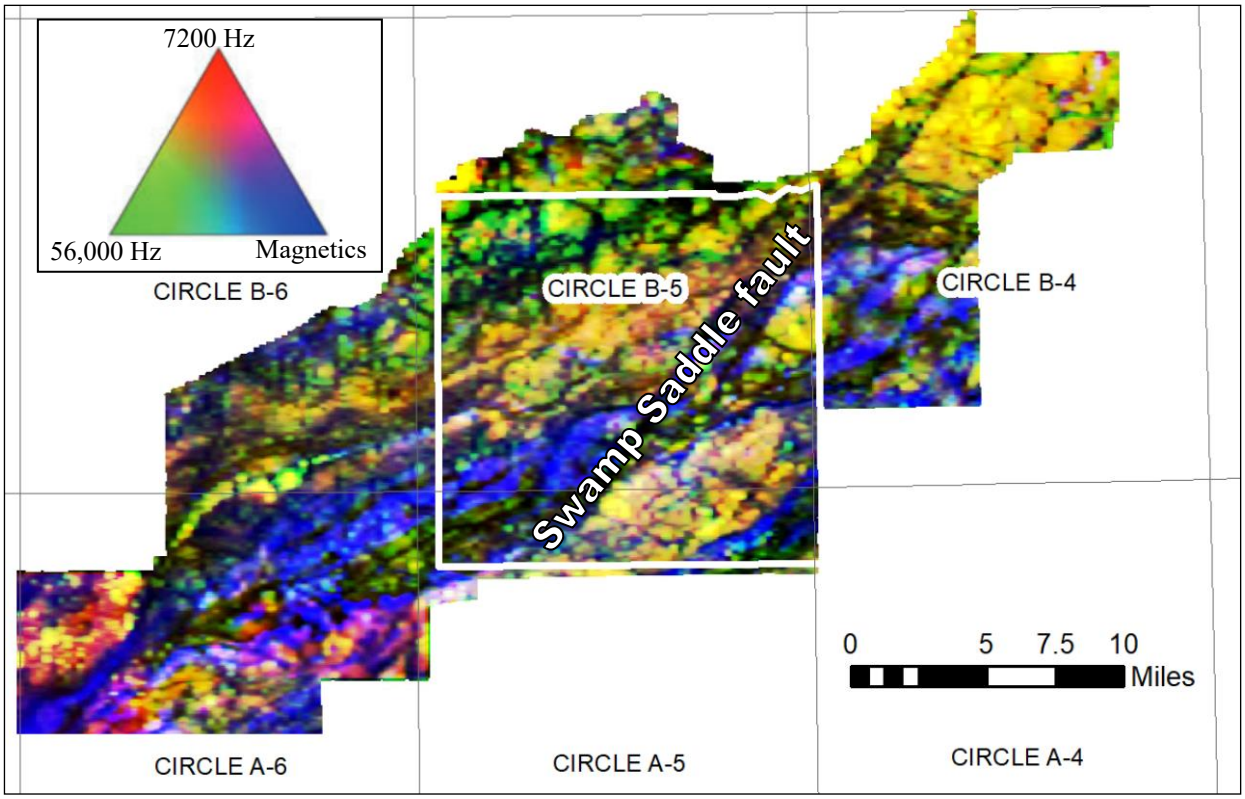

Figure 1. Multi-band raster for visualization of the geophysical survey covering the map area (Burns and others, 2006). 7200 Hz resistivity is assigned to the red band, 56,000 Hz resistivity to green, and magnetics to blue. Areas of black are low in all three datasets (conductive, low magnetic values). Areas of yellow have high resistivity in both 7200 Hz and 56,000 Hz datasets and low magnetic values. Areas of blue have elevated magnetic values and are conductive. The border of the study area is shown by a white line.

the study area. Additional interpretation of geophysical data, photointerpreted linears, and field mapping show units to be offset left-laterally along multiple, subsidiary, northeast-trending, high-angle faults. A zone of high conductivity along the northern boundary of the map area correlates with recessively weathering, graphite-bearing schist (unit €Zg).

Lode and Placer Mineralization

The study area falls within a northeast-oriented trend of plutonic-related mineralization in the central and southwestern Fairbanks mining district and the placer gold district in the northwest portion of the Circle mining district. Compiled information on mineralization (U.S. Geological Survey, 1996), proprietary industry mineral exploration data, and data from this study suggest that lode and placer gold and polymetallic occurrences in the geologic mapping area may be related to plutonic hydrothermal systems like those responsible for mineralization in the Fairbanks mining district and larger Tintina Gold Belt (also known as the Tintina Gold Province; Gough and Day, 2007). As of 2007, two placer operations were active within the study area and many of the drainages are still claimed in 2022. The area has also been explored for lode gold over the past few decades by exploration companies and prospectors. Geoinformatics Exploration Inc. acquired the Hope Creek lode exploration property from Kennecott Exploration Company in 2005 (Geoinformatics Exploration Inc., 2005). According to the news release, prior work on the

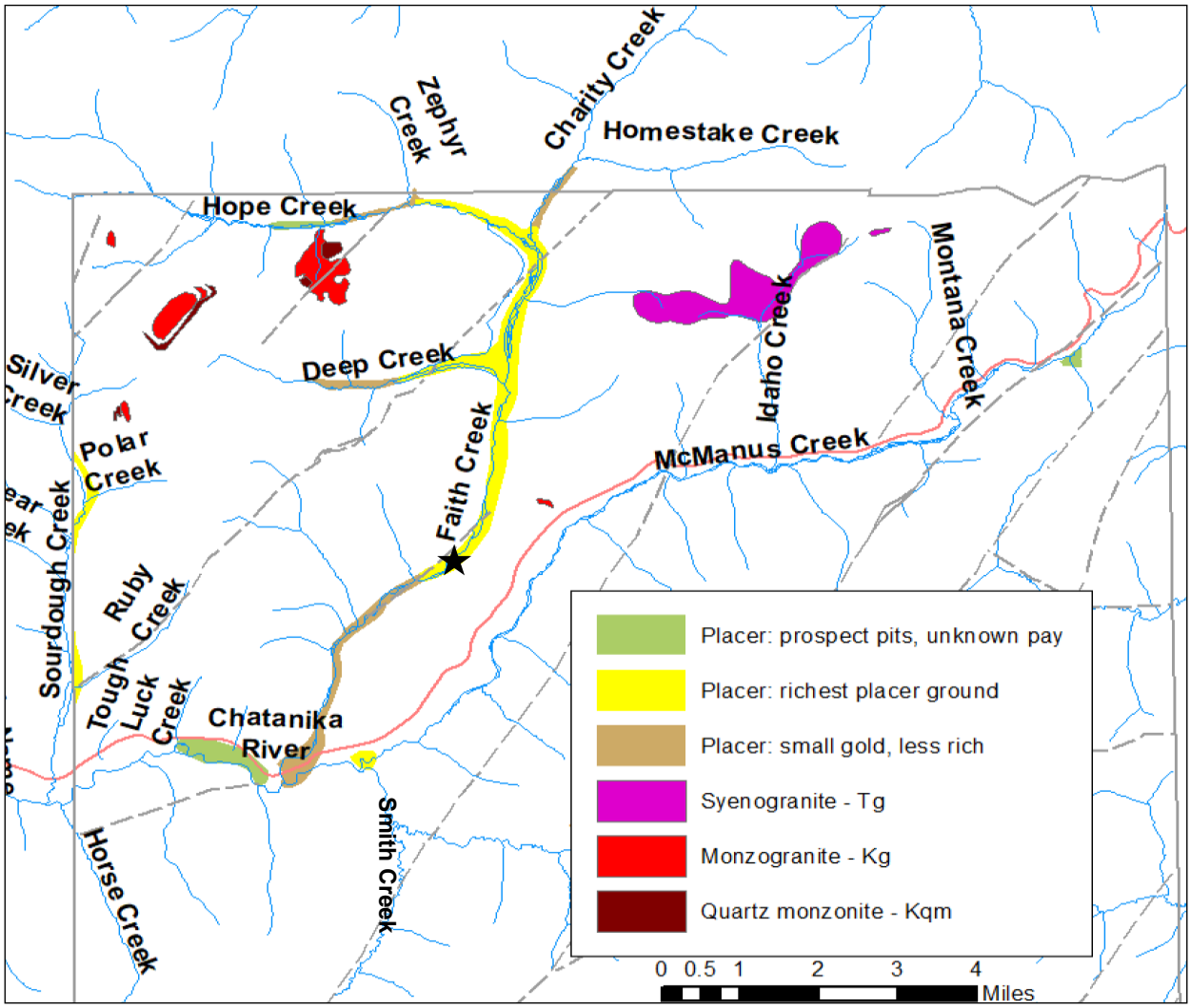

Figure 2. Significant placer gold workings and igneous bodies in the northern two-thirds of the study area. Map also shows faults (dashed lines), the study area boundary (gray line), and Steese Highway (red line). Below Deep Creek's confluence with Faith Creek, crystalline gold and quartz-gold nuggets were recovered by placer miners (De Anne Stevens, pers. commun., 2007), implying a nearby lode source. Below this stretch of stream, placer gold increases in fineness as it travels further away from the lode source. Black star is approximate location of "yellow clayey material" (fault gouge?) uncovered during placer mining operations.

lode property in 1999–2000, likely by Kennecott Exploration Company, included six reverse circulation drill holes and a helicopter-borne aeromagnetic and radiometric survey. In 2016, Kinross Gold USA, Inc. acquired claims in the area and subsequently transferred ownership in 2020 to Golden Circle Resources, Inc., whose company contact information is Great American Minerals Exploration, Inc. (Alaska Department of Natural Resources, 2022). Exploration information generated on the claims by Kinross and Golden Circle is not publicly available. Golden Circle continues to hold mining claims for lode exploration north and south of Deep Creek as of 2022.

Placer gold in Faith, McManus, and other creeks is likely eroded from lode sources associated with variably porphyritic Cretaceous monzogranite, quartz monzonite, and other bodies of

similar composition (units Kg and Kqm; fig. 2). Igneous samples with major-element geochemical data were assigned rock names based on the methodology described in appendix A to help define the units. The quartz monzonite bodies form discreet plugs, dikes, and sills peripheral to the monzogranite stocks. The quartz monzonite contains coarse-grained biotite and hornblende and have previously been called lamprophyre (Smith and others, 1987). Three types of mineralization are associated with the Cretaceous intrusions: arsenopyrite–pyrite–quartz–sericite–carbonate veins and boxworks; pervasive sericite–pyrite–arsenopyrite alteration of the intrusion; and semi-massive stibnite–quartz veins. A Tertiary porphyritic syenogranite body also crops out in the northern map area. A sample of fractured, hornfelsed quartzite from the margin of the Tertiary pluton contained 1.045 ppm Au (Athey and others, 2008).

Although gold placers in the Faith Creek drainage appear to correlate with the monzogranite suite, their relationship is not straightforward. On Hope and Deep creeks, the richest producing placers start significantly downstream from the igneous bodies themselves, suggesting that the bulk of the gold might be in the country rock or in structures proximal to the intrusions. Lower Deep Creek contained the richest pay in the area (De Anne Stevens, pers. commun., 2007). There is no change in the modern gradients of the streams to account for the distribution of the placer gold. Geoinformatics Exploration Inc. (2005) described the mineralization and geology as a gold–arsenic–antimony anomaly associated with structurally controlled intrusions and gold-rich shears and faults, further suggesting that "all [historical] coarse placer gold distribution appears to relate to monzonite intrusions in the district." The monzonite mentioned in the press release likely refers to the genetically related monzogranite (unit Kg) and quartz monzonite (unit Kqm) intrusions described below.

The placer deposits are likely not far removed from the lode source of the gold, since crystalline gold and gold with quartz are found in middle Faith Creek (fig. 2; De Anne Stevens, pers. commun., 2007). Lower on Faith Creek and below a section of prominent "yellow clayey material" (likely fault gouge), placer gold fineness is reported to increase and gold content and grain size drop dramatically, making the pay not as rich. Other creeks and creek sections with lesser amounts of gold and poor production include upstream on Hope and Deep creeks and Charity and Homestake creeks.

Faith Creek valley is a broad, flat bedrock valley with incised paleochannels sub-parallel to the current valley trend; gravels and cover are/were comparatively thin and therefore placer deposits were not deeply buried (De Anne Stevens, pers. commun., 2007). Discontinuous high-level terraces with gravel along Faith Creek are nearly 300 feet above modern stream level. Aerial photographs indicate the high-level terraces continue on the east side of Faith Creek valley from Deep Creek's confluence to as far south as where Faith Creek turns to the southwest (Stevens, 2011).

The Chatanika River and McManus Creek valley bisects the study area roughly from east to west; McManus Creek flows into the Chatanika River at the confluence of Smith Creek. As of 2007, placer miners were actively and continually mining with good success using small suction dredges at the mouth of Smith Creek (De Anne Stevens, pers. commun., 2007). Minor mining activity was also noted on a small, north-flowing, unnamed tributary to McManus Creek in the northeast part of the study area (productivity unknown). Placer mining along the Sourdough Creek drainage was extensive; the extent and volume of placer tailings suggest this area was very

productive. Details of these workings are described in the Alaska Resource Data File (U.S. Geological Survey, 1996).

High-level terraces flank the main Chatanika River–McManus Creek drainage in the lower reaches of the field area (Stevens, 2011). Lower Sourdough Creek has the most extensive high-level terrace system in the field area, with up to three levels evident (most just outside of field area); the highest terraces are more than 100 feet above modern stream level. Whether the terraces are gold-bearing is unknown; some are capped with gravel and very extensive (De Anne Stevens, pers. commun., 2007).

IGNEOUS UNIT DESCRIPTIONS

Tg PORPHYRITIC SYENOGRANITE (Tertiary) — Fine- to very fine-grained, porphyritic-textured hypabyssal syenogranite stocks are present in the northern third of the map area. Light brown to white weathering, white to light gray to pink colored. Porphyritic intrusions contain widely varying proportions of clear to gray quartz, feldspar, and ± biotite phenocrysts (<30 percent) in an aphanitic to finely granular (0.2 mm) matrix. Found adjacent to the pluton, sample 07MBW415A of fractured, hornfelsed quartzite with pyrrhotite and (or) a dark-red, crystalline, hematite-coated quartz druse contained 1.045 ppm Au (Athey and others, 2008). Major- and minor-oxide and trace-element analyses indicate the granite intrusions are rift-related and formed in an extensional tectonic setting (fig. B1). Magnetic susceptibility is generally low to moderate (0.05–1.14, averaging 0.33 x 10^{-3} Système International [SI]). Unit yielded an $^{40}Ar/^{39}Ar$ biotite plateau age of 56.8 ± 0.2 Ma (map location A1; appendix E).

Kg MONZOGRANITE (Cretaceous) — Coarse- to very fine-grained, porphyritic-textured, lesser equigranular-textured hypabyssal monzogranite (dominant) to granodiorite dikes and stocks are present in the northern half of the map area. White weathering, white to gray colored. Porphyritic intrusions contain widely varying proportions of clear to gray quartz, feldspar, biotite (unless altered), and ± hornblende (<30 percent mafic minerals) phenocrysts. Groundmass of porphyritic variety is aphanitic to finely granular; light tan, gray, or green. Occasionally contains red, clear, glassy euhedral garnets as phenocrysts or xenocrysts incorporated from host metamorphic rocks. Host rocks surrounding the intrusions are locally hornfelsed and silicified. Intrusions are chloritized and rarely intensely sericitized ± carbonate alteration. Associated mineralization includes pyrite, pyrrhotite, arsenopyrite, and stibnite and secondary scorodite and stibiconite. Sericite from hydrothermally altered sample 07JEA299A yielded a maximum age of about 86 Ma before resetting to 72 Ma (plateau reset age of 72.1 ± 0.04 Ma [map location A2]; appendix E). The granite–granodiorite intrusions have an island-arc, trace-element signature and are subduction-related (fig. B1). Magnetic susceptibility is generally low (0.05–0.15, averaging 0.11 x 10^{-3} SI). Unit yielded an $^{40}Ar/^{39}Ar$ biotite plateau age of 91.2 ± 0.3 Ma (map location A3; appendix E).

Kqm QUARTZ MONZONITE (Cretaceous) — Medium- to coarse-grained, porphyritic-textured, lesser equigranular-textured hypabyssal quartz monzonite, minor granodiorite and tonalite, and rare diorite dikes and stocks are present in the northern half of the map area. Brown to olive-brown weathering, light greenish-gray to dark gray colored. Intrusions con-

tain widely varying proportions of quartz, feldspar, ± biotite, and ± hornblende phenocrysts (<25 percent mafic minerals) in an aphanitic to finely granular matrix. Occasionally contains red, clear, glassy euhedral garnets (xenocrysts?) and xenoliths incorporated from host metamorphic rocks. The granite intrusions are locally chlorite-, carbonate-, and sericite-altered. Associated mineralization includes pyrite, pyrrhotite, arsenopyrite, and stibnite and secondary scorodite and stibiconite. The intrusions have an island-arc, trace-element signature and are subduction-related (fig. B1). Magnetic susceptibility is generally low (0.10–0.45, averaging 0.19 x 10^{-3} SI). Granodiorite yielded an $^{40}Ar/^{39}Ar$ hornblende plateau age of 92.5 ± 0.5 Ma (map location A4; app. E).

METAMORPHIC HISTORY AND REGIONAL CORRELATIONS

Metamorphic rocks in the field area were differentiated into five similar but coherent packages based on field observations, compositional data, and geophysical signature: (1) Ꞓ€Zgq—Occasionally graphitic (generally <1 percent carbon) quartzite and schist commonly containing a bimodal grain size of fine-grained quartz and a larger-sized population of relict quartz and feldspar grains (described as containing "grit" grains) and lesser Ꞓ€Zg—Graphitic schist and quartzite; (2) Ꞓ€Zcs—Calcareous garnet-rich quartzite and schist with arc-related metamafic rocks and rare marble; (3) Ꞓ€Zqs—Fine-grained quartzite and schist containing quartz and feldspar grit grains and associated extension-related metabasalt (unit KZa) that may represent a later igneous event; (4) Ꞓ€Zq—Fine-grained quartzite commonly containing quartz and feldspar grit grains; and (5) Ꞓ€Zs—Schist and quartzite commonly containing quartz and feldspar grit grains. In this mapping, we define "grit" as a component of the rock, for example, the relict coarse fraction of a bimodal metasedimentary rock such as Ꞓ€Zgq summarized above, rather than a lithology, as in "a sandstone composed of particles of conspicuously unequal sizes (including small pebbles or gravel)" in Neuendorf and others (2011; definition [d]). In the study area, quartz schist + quartzite are about twice as abundant as mica schist + semischist + calcareous schist + metamafic rocks. Unit contacts trend east–northeast and appear to be offset left-laterally (and vertically?) along northeast-trending, high-angle faults.

Units in the field area are generally correlative with other Yukon-Tanana upland metamorphic rocks, as evidenced by similar metamorphic facies and trends, compositions, and Proterozoic to later Archean detrital zircon ages (Newberry and others, 1996; Bradley and others, 2007), including metamafic rocks (unit KZa) that have similar major- and trace-element compositions to Fairbanks mining district within-plate amphibolites (Newberry and other, 1996). Pressure–temperature data indicate peak metamorphism in the study area straddled the greenschist and epidote–amphibolite facies boundary on the lower end and approached the epidote–amphibolite- and amphibolite-facies boundary at 9 kbar and 600 °C on the upper end (app. D). Although the highest published pressures and temperatures from the Fairbanks area amphibolite-facies schist (7.5 kbar and 550 °C; Joy and others, 1996) are lower than those calculated for the study area, Douglas and others (2002) suggest similar peak metamorphic conditions for Fairbanks at about 10 kbar and 600 °C. No eclogite-facies rocks were identified in the study area and our mapping did not confirm Chatanika terrane schist and quartzite along the Steese Highway east of Sourdough Creek (Foster and others, 1983). Local pressure and temperature indicators do show a general increase in metamorphic grade to the northwest, although this is complicated by faulting.

The latest metamorphic event occurred prior to or around 140–148 Ma, based on an $^{40}Ar/^{39}Ar$ hornblende cooling age of 144 ± 4 Ma (schist from unit €Zq [map location A6]; app. E). The argon closure temperature of hornblende (500 °C) is close to the average of temperatures calculated for garnet–biotite pairs in the study area (460–600 °C). Similarly, Douglas and others (2002) report hornblende from Fairbanks schist cooled to the hornblende closure temperature at 150 Ma. Unlike the pervasive greenschist retrograde metamorphism present in the Fairbanks area (Newberry and others, 1996), garnet and hornblende-rimmed actinolite grains in the study area show a prograde metamorphic trend uncomplicated by retrograde alteration. The localized, retrograde greenschist-metamorphic event in the Fairbanks area, which occurred from 100–115 Ma, is bracketed by the overthrust of the eclogite (115–140 Ma) and pluton emplacement with mineralizing hydrothermal activity (~90 Ma), according to ages from Douglas and others (2002) defining these three events. Fluids associated with both or either bracketing event could have been responsible for the retrograde greenschist-facies metamorphism. Conversely, the lack of low-angle structures and eclogite-facies rocks and relative scarcity of mineralization and plutons in the study area as compared to other parts of the Fairbanks mining district could account for its straightforward, prograde metamorphic history.

The study area's abundant quartz and feldspar grit, associated metagraywacke (in unit €Zcs), and other rare, preserved sedimentary textures such as rip-up clasts suggest correlation with the greenschist-facies, Cambrian to Late Proterozoic Wickersham Grit unit in the Livengood and Circle quadrangles (Foster and others, 1983; Weber and others, 1988, 1992). Grit-bearing quartzite or schist was observed at about 20 percent of field stations. Detrital zircon ages from presumed Wickersham Grit equivalents in the Tanana Quadrangle (unit PzPws [?] in Reifenstuhl and others, 1997) and in the Talkeetna Quadrangle north of the Denali Fault (unit Pzsv in Reed and Nelson, 1980) show similar peaks to a grit-bearing quartzite sample from unit €Zq (peaks at 1272, 1826, 1967, 2334, and 2691 Ma; app. F; comparative detrital zircon data from Bradley and others, 2007). The youngest zircon grains from the samples are 1198 Ma from the Wickersham unit (Tanana Quadrangle), 1789 Ma from the grit-bearing Yukon–Tanana unit (Talkeetna Quadrangle), and 946 Ma from unit €Zq.

The main protolith of the metamorphic rocks are likely siliciclastic sediments shed from a continental source, for example, a North American provenance. Bradley and others (2007) support a North American (Laurentian) source for the detrital zircon grains. Potential depositional environments range from marine deep water to shelf. Granule-size grit, rip-up clasts, and the presence of carbonate suggest transport offshore and deposition above the carbonate compensation depth (fig. 3). Relict hummocky cross-beds support a proximal shelf environment and trace to low percentages of graphite indicate the protolith included beds with organic material, requiring a proximal source of organic matter. Metamafic rocks record deposition of sediments (described as graywacke) derived at least partly from mafic volcaniclastic sediments or eroded igneous rocks in a similar range of environments.

METAMORPHIC UNIT DESCRIPTIONS

KZa AMPHIBOLITE (Early Cretaceous–Late Proterozoic) — Fine- to medium-grained, schistose to semi-schistose, metamorphosed mafic dikes or sills. Dark gray-green colored. Mineral content varies depending on chemical composition and metamorphic grade of the

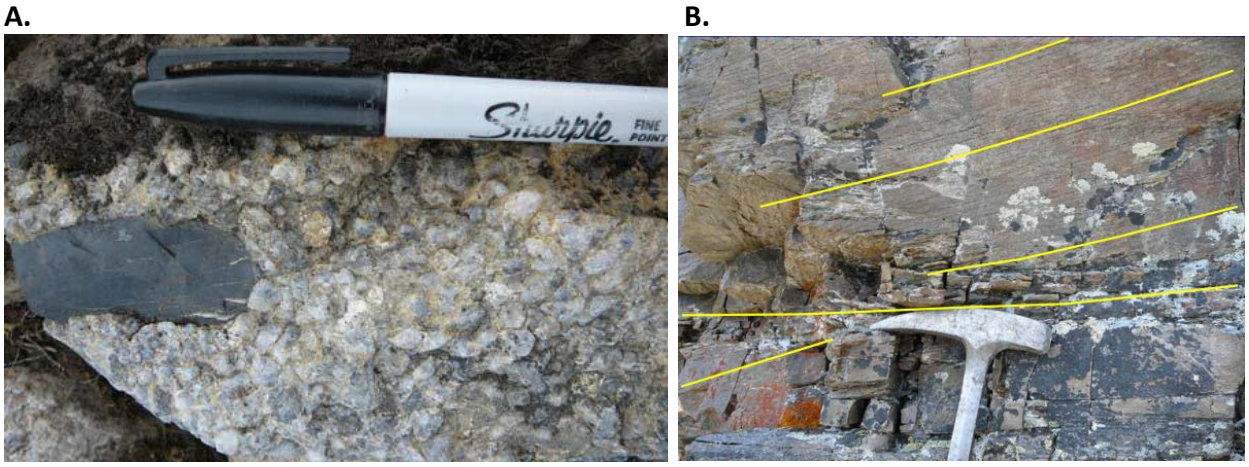

Figure 3. The southern grit unit (Mt. Ryan area) contains the highest percentage of grit and rare granule conglomerate. **A.** One location also contained an argillite clast, interpreted as a rip-up clast. **B.** The only other relict sedimentary features observed included possible cross bedding and graded bedding. Bedding thickness ranges widely from several centimeters to 10's of meters.

rock, but may include chlorite, plagioclase, hornblende, actinolite, garnet, epidote, clinozoisite, carbonate, magnetite, and (or) pyrite. Major- and minor-oxide and trace-element analyses indicate the rocks are rift-related and formed in an extensional tectonic setting (fig. B2). Magnetic susceptibility is generally moderate (0.29–0.51, averaging 0.42 x 10^{-3} SI). Metamafic unit is found interfoliated primarily with unit €Zqs; contacts may represent either an ancient intrusive or stratigraphic relationship with unit €Zqs. Upper limit of age is based on spatial association with unit €Zq. Given the possibility of an ancient intrusive relationship with unit €Zqs, the lower age is defined by the age of cooling following the last regional metamorphism ($^{40}Ar/^{39}Ar$ hornblende age pseudo-plateau of 144 ± 4 Ma; semischist from unit €Zq [map location A6]; app. E).

€Zgq GRAPHITIC QUARTZITE, GRIT-BEARING QUARTZITE, AND QUARTZOSE SCHIST (Cambrian–Late Proterozoic) — Very fine- to fine-grained, sucrosic, variably graphitic quartzite > grit-bearing quartzite > quartzose schist. White- to gray-colored outcrops are either platy-breaking or hard and massive depending on the mica content of the rock. Quartzite and schist are interfoliated on a scale of several centimeters to several meters. Composition varies but is generally quartz, white mica, plagioclase, albite, garnet, calcite, biotite, chlorite, and tourmaline. About 20 percent of the unit contains coarse to very coarse, subangular to subrounded, relict sand grains or "grit" grains of quartz and feldspar in a very fine- to medium-grained quartz sand matrix. Where present, grit grains generally average 3 percent of the rock, but may rarely comprise up to 70 percent. Grit grains are generally 2 mm in diameter, but up to 1 cm in diameter. Unit occasionally contains <1 percent graphite and is conductive (Burns and others, 2006). Magnetic susceptibility is generally low (0.02–0.25, averaging 0.12 x 10^{-3} SI); quartzite and metagrit generally have lower magnetic susceptibilities than schist. Age is based on spatial association with unit €Zq.

€Zg GRAPHITIC SCHIST AND QUARTZITE (Cambrian–Late Proterozoic) — Fine- to medium-grained, weakly graphitic schist > quartzite > semischist. Light brown or light gray- to black-colored, platy-breaking or hard and massive outcrops. Unit appears to recessively weather; less competent rocks containing more mica and graphite may be more than prevalent than competent float suggests. Unit also appears along a fault and may be enriched in graphite. Composition varies but is generally quartz, white mica (5–15 percent), plagioclase (20–40 percent), garnet (2–10 percent), calcite (<15 percent), and chlorite, with up to 1.16 percent graphite (appendix C). Unit is anomalously conductive (Burns and others, 2006) and does not contain any grit-bearing quartzite or schist. Magnetic susceptibility is generally low (0.05–0.20, averaging 0.12 x 10^{-3} SI). Age is based on spatial association with unit €Zq.

€Zcs CALCAREOUS SCHIST AND QUARTZITE, FELDSPATHIC QUARTZITE, AND AMPHIBOLITE (Cambrian–Late Proterozoic) — Very fine- to fine-grained, sucrosic calcareous schist and quartzite, lesser feldspathic quartzite and mica-rich schist, uncommon amphibolite, and rare, thin beds of marble. Brown-weathered, carbonate-rich schist forms topographic lows, and outcrops are platy and friable. Rocks are more competent and massive or semi-schistose with increasing quartz and feldspar content. In a few locations, carbonate content increases to form rare, thin (<0.5 m thick), massive beds of gray to brown-gray, crystalline marble and impure marble. Composition is dominantly quartz, white mica, calcite (<15 percent), garnet (~10 percent), feldspar (plagioclase + albite are <10 percent), biotite, chloritoid, tourmaline, and one possible instance of staurolite. This unit contains significantly more garnet and carbonate than the other metamorphic units in the package, and the only chloritoid and staurolite; mineralogical differences are due to its chemical composition, not changes in metamorphic grade. Unit does not contain any grit-bearing quartzite or schist, and contains less graphite than any of the other metamorphosed sedimentary units. Unit is resistive (Burns and others, 2006). Magnetic susceptibility is generally low (0.04–0.39, averaging 0.21 x 10^{-3} SI); quartzite and schist have similar magnetic susceptibilities, although rare schist outliers measure up to 12.5 x 10^{-3} SI. Age is based on spatial association with unit €Zq.

Fine-grained, gray-green to gray amphibolite and mafic schist occur as discrete layers within the quartzite and schist lithologies of unit €Zcs and are not recognized elsewhere in the study area. Mineral content varies depending on chemical composition and metamorphic grade of the rock, but may include chlorite, plagioclase, hornblende, actinolite, garnet, epidote, clinozoisite, carbonate, magnetite, tourmaline, pyrrhotite, and (or) pyrite. Presence of tourmaline in about half of the samples indicates a sedimentary protolith (greywacke likely derived from a mafic igneous source), instead of a mafic igneous protolith. The rocks (protolith of the greywacke) have an island-arc, trace-element signature (fig. B2). Magnetic susceptibility is generally moderate (0.16–0.62, averaging 0.42 x 10^{-3} SI). Age is based on spatial association with unit €Zq.

€Zqs QUARTZITE, QUARTZOSE SCHIST, AND MARBLE (Cambrian–Late Proterozoic) — Very fine- to fine-grained, sucrosic quartzite > grit-bearing quartzite and quartzose schist. White- to gray-colored outcrops are either platy-breaking or hard and massive depending on the mica content of the rock. Quartzite and schist are interfoliated on a scale of several centimeters

to 10's of meters. Composition varies but is generally quartz, white mica, plagioclase, albite, garnet, calcite, biotite, chlorite, and tourmaline. About 10 percent of the unit contains coarse to very coarse, subangular to subrounded, relict sand grains or "grit" grains of quartz and feldspar in a very fine- to medium-grained quartz sand matrix. Unit locally contains graphite and is moderately conductive (Burns and others, 2006). Magnetic susceptibility of quartzite and schist is low (0.02–0.23, averaging 0.17 x 10^{-3} SI), with rare mafic schist measuring up to 11.34 x 10^{-3} SI; the airborne geophysical signature of this unit varies widely, possibly due to the presence of non-outcropping unit KZa layered within the quartzite and schist (Burns and others, 2006). Age is based on spatial association with unit €Zq.

One locality of white, medium-grained, crystalline marble, impure marble, and calcareous schist located in the southwestern corner of the map. Lithologies form an unusual, northwest-trending, topographically low, steep, narrow ridge about 1,000 feet long on the north side of Frozenfoot Creek that truncates abruptly at each end. The small ridge is mapped as an anticline. Lithologies are located adjacent to the Swamp Saddle fault and may be a transported fault sliver. There are no other occurrences of this distinctive lithology in the map area. Magnetic susceptibility is low. Age is based on spatial association with unit €Zq.

€Zq QUARTZITE AND GRIT-BEARING QUARTZITE (Cambrian–Late Proterozoic) — Fine-grained, sucrosic, quartzite-dominant unit: quartzite > grit-bearing quartzite >> micaceous quartzite > schist. Quartzite and schist are interfoliated on a scale of several centimeters to 10's of meters. Layering may represent original bedding. One locality showed possible relict cross bedding. Composition varies but is generally quartz, white mica, plagioclase, albite, garnet, calcite, biotite, chlorite, and tourmaline. About 20 percent of the unit contains coarse to very coarse, subangular to subrounded, relict sand grains or "grit" grains of quartz and feldspar in a very fine- to medium-grained quartz sand matrix. Where present, grit grains generally average 5 percent of the rock, but may rarely comprise up to 70 percent. Grit grains are generally 2 mm in diameter, but up to 1 cm in diameter. One locality of pebble conglomerate with mudstone rip-up clasts occurs on Mt. Ryan in the south-central portion of the study area. Unit locally contains graphite but is generally resistive (Burns and others, 2006). Magnetic susceptibility is generally low (0.02–0.24, averaging 0.23 x 10^{-3} SI), with rare mafic schist measuring up to 35 x 10^{-3} SI. Age is based on detrital zircon data (metasandstone with up to 70 percent grit grains [map location DZ1]; appendix F) and correlation with the Wickersham Grit unit in the Circle and Livengood quadrangles (Cambrian trace fossil Oldhamia; Foster and others, 1983; Weber and others, 1988).

€Zs QUARTZOSE SCHIST, MICA-RICH SCHIST, AND GRIT-BEARING QUARTZITE (Cambrian–Late Proterozoic) — Very fine- to fine-grained quartz schist >> grit-bearing quartzite > quartzite > mica-rich schist. White- to gray-colored outcrops are either platy-breaking or hard and massive depending on the mica content of the rock. Composition varies but is generally quartz, white mica, plagioclase, albite, garnet, biotite, chlorite, tourmaline, and magnetite. Grit-bearing quartzite contains 1–20 percent grit grains, averaging 8 percent. Magnetic susceptibility is low (0.02–0.15, averaging 0.07 x 10^{-3} SI); schist-dominant areas have a higher magnetic signature (Burns and others, 2006). Unit is generally conductive (Burns and others, 2006). Age is based on loose spatial association with unit €Zq.

ACKNOWLEDGMENTS

This project is part of the State of Alaska's Airborne Geophysical/Geological Mineral Inventory (AGGMI) program, a special multi-year investment by the state to expand Alaska's geologic and mineral resources knowledge base, catalyze future private-sector mineral exploration and development, and guide state planning. AGGMI was funded by the Alaska State Legislature and managed by State of Alaska, Department of Natural Resources, Division of Geological & Geophysical Surveys. This geologic map was funded in part by the USGS National Cooperative Geologic Mapping Program under STATEMAP award number 07HQAG0076, 2007 (fieldwork), and G20AC00367, 2020 (GeMS conversion). Additional funding was provided by the State of Alaska General Fund. The views and conclusions contained in this document are those of the authors and should not be interpreted as necessarily representing the official policies, either expressed or implied, of the U.S. Government.

The authors thank student intern Liping Jing for her help in the field and afterwards with the field notes database. We also thank Sean Regan and our reviewer Evan Twelker, whose helpful comments increased the quality of the map and report.

REFERENCES

Alaska Department of Natural Resources, 2022, Land Administration System, last accessed July 27, 2022. http://dnr.alaska.gov/projects/las/

Athey, J.E., Freeman, L.K., Werdon, M.B., Szumigala, D.J., Lessard, R.R., Newberry, R.J., Hansen, S.E., and Jing, L., 2008, Major-oxide, minor-oxide, and trace-element geochemical data from rocks and stream sediments collected in the northern Fairbanks mining district, Circle Quadrangle, Alaska in 2007: Alaska Division of Geological & Geophysical Surveys Raw Data File 2008-1 v. 1.0.1, 41 p. https://doi.org/10.14509/15901

Benowitz, J.A., Layer, P.W., and Freeman, L.K., 2011, 40Ar/39Ar ages from the east Bonnifield geologic map area, Fairbanks A-1, Fairbanks A-2, Healy D-1, and Healy D-2 quadrangles, Alaska: Alaska Division of Geological & Geophysical Surveys Raw Data File 2011-2 v. 1.1, 22 p. https://doi.org/10.14509/22482

Bradley, D.C., McClelland, W.C., Wooden, J.L., Till, A.B., Roeske, S.M., Miller, M.L., Karl, S.M., and Abbott, J.G., 2007, Detrital zircon geochronology of some Neoproterozoic to Triassic rocks in interior Alaska, *in* Ridgway, K.D., Trop, J.M., Glen, J.M.G., and O'Neill, J.M., eds., Tectonic Growth of a Collisional Continental Margin: Crustal Evolution of Southern Alaska: Geological Society of America Special Paper 431, p. 155–189. https://doi.org/10.1130/2007.2431(07)

Brown, E.H., and Forbes, R.B., 1986, Phase petrology of eclogitic rocks in the Fairbanks district, Alaska, in Evans, B.W., and Brown, E.H., eds., Blueschists and eclogites: Geological Society of America, Memoir 164, p. 155–167.

Burns, L.E., Fugro Airborne Surveys Corp., and Stevens Exploration Management Corp., 2006, Line, grid, and vector data and plot files for the airborne geophysical survey data of northeast Fairbanks area, Fairbanks and Circle mining districts, interior Alaska: Alaska Division of Geological & Geophysical Surveys Geophysical Report 2006-3, 21 sheets, 1 DVD. https://doi.org/10.14509/14522

Burns, L.E., Graham, G.R.C., Barefoot, J.D., Fugro Airborne Surveys, and Stevens Exploration Management Corp., 2019a, Northeast Fairbanks electromagnetic and magnetic airborne

geophysical survey data compilation: Alaska Division of Geological & Geophysical Surveys Geophysical Report 2018-11, 12 p. https://doi.org/10.14509/30062

Burns, L.E., Graham, G.R.C., Barefoot, J.D., Woods, Rebecca-Ellen, Dighem, WGM, Inc., Fugro Airborne Surveys, and Stevens Exploration Management Corp., 2019b, Fairbanks electromagnetic and magnetic airborne geophysical survey data compilation: Alaska Division of Geological & Geophysical Surveys Geophysical Report 2019-18, 13 p. https://doi.org/10.14509/30230

Chang, Z., Vervoort, J.D., McClelland, W.C., and Knaack, C., 2006, U-Pb dating of zircon by LA-ICP-MS: Geochemistry, Geophysics, Geosystems, v. 7, n. 5, 14 p.

De la Roche, H., Leterrier, J., Grandclaude, P. and Marchal, M., 1980, A classification of volcanic and plutonic rocks using R1-R2 diagrams and major element analyses—its relationships with current nomenclature: Chemical Geology, v. 29, p. 183–210.

Deer, W.A., Howie, R.A., and Zussman, J., 1997, Rock-Forming Minerals: Double Chain Silicates, 2nd edition, Oxford, United Kingdom, Alden Press, Osney Mead, v. 2B, 758 p.

Douglas, T.A., Layer, P.W., Newberry, R.J., and Keskinen, M.J., 2002, Geochronologic and thermobarometric constraints on the metamorphic history of the Fairbanks Mining District, western Yukon-Tanana terrane, Alaska: Canadian Journal of Earth Science v.39, p. 1107–1126.

Foster, H.L., Laird, Jo, Keith, T.E.C., Cushing, G.W., and Menzie, D.W., 1983, Preliminary geologic map of the Circle Quadrangle, Alaska: U.S. Geological Survey Open-File Report 83-170-A, 30 p., 1 sheet, scale 1:250,000. https://dggs.alaska.gov/pubs/id/12617

Geoinformatics Exploration Inc., 2005, News release, August 29, 2005, Geoinformatics Announces the Acquisition of Four Properties in Alaska and British Columbia and Provides Update on the Tasmanian, New Zealand and Sanatana Project: last accessed via the web archive on July 8, 2022. https://web.archive.org/web/20051226035118/http://www.geoinformex.com/content/news_press_releases/Cordilleran_Aug29.pdf

Gough, L.P., and Day, W.C., 2007, Tintina gold province study, Alaska and Yukon Territory, 2002-2007: U.S. Geological Survey Fact Sheet 2007-3061, 4 p. https://doi.org/10.3133/fs20073061

Irvine, T.N., and Baragar, W.R.A., 1971, A guide to the chemical classification of the common volcanic rocks: Canadian Journal of Earth Sciences, v. 8, p. 523–548.

Joy, B.R., Keskinen, M.J., and Newberry, R.J., 1996, Preliminary thermobarometry and microprobe mineral compositions, Fairbanks area schists and amphibolites: Alaska Division of Geological & Geophysical Surveys Public Data File 96-12, 15 p. https://doi.org/10.14509/1736

Layer, P.W., Drake, Jeffrey, and Athey, J.E., *in prep.*, $^{40}Ar/^{39}Ar$ data from the northern Fairbanks mining district, Circle Quadrangle, Alaska: Alaska Division of Geological & Geophysical Surveys Raw Data File.

Meschede, Martin, 1986, A method of discriminating between different types of mid-ocean ridge basalts and continental tholeiites with the Nb–Zr–Y diagram: Chemical Geology, v. 56, p. 207–218.

Neuendorf, K.K.E., Mehl, J.P., Jr., and Jackson, J.A., eds., 2005, Glossary of geology (5th ed.; online subscription): Alexandria, Va., American Geological Institute, 799 p.

Newberry, R.J., Bundtzen, T.K., Clautice, K.H., Combellick, R.A., Douglas, Tom, Laird, G.M., Liss, S.A., Pinney, D.S., Reifenstuhl, R.R., and Solie, D.N., 1996, Preliminary geologic map of the Fairbanks mining district, Alaska: Alaska Division of Geological & Geophysical Surveys Public Data File 96-16, 17 p., 2 sheets, scale 1:63,360. https://doi.org/10.14509/1740

O'Sullivan, P.B., and Athey, J.E., in prep., U-Pb detrital zircon geochronology of a Cambrian–Late Proterozoic quartzite in the northern Fairbanks mining district, Circle Quadrangle, Alaska: Alaska Division of Geological & Geophysical Surveys Raw Data File.

Pearce, J.A., Harris, N.B.W., and Tindle, A.G., 1984, Trace element discrimination diagrams for the tectonic interpretation of granitic rocks: Journal of Petrology, v. 25, p. 956–983.

Reed, B.L., and Nelson, S.W., 1980, Geologic map of the Talkeetna Quadrangle, Alaska: U.S. Geological Survey Miscellaneous Investigations Series Map 1174, 15 p., 1 sheet, scale 1:250,000. https://dggs.alaska.gov/pubs/id/12942

Reifenstuhl, R.R., Dover, J.H., Newberry, R.J., Clautice, K.H., Liss, S.A., Blodgett, R.B., Bundtzen, T.K., and Weber, F.R., 1997, Interpretive geologic bedrock map of the Tanana B-1 Quadrangle, central Alaska: Alaska Division of Geological & Geophysical Surveys Report of Investigation 97-15B, 15 p., 1 sheet, scale 1:63,360. https://doi.org/10.14509/2552

Smith, T.E., Pessel, G.H., and Wiltse, M.A., eds., 1987, Mineral assessment of the Lime Peak-Mt. Prindle area, Alaska: Alaska Division of Geological & Geophysical Surveys Miscellaneous Publication 29, 712 p., 13 sheets, scale 1:63,360. https://doi.org/10.14509/731

Steiger, R.H., and Jaeger, E., 1977, Subcommission on geochronology: Convention on the use of decay constants in geo and cosmochronology: Earth and Planet Science Letters, v. 36, p. 359–362.

Stevens, D.S.P., 2011, Surficial-geologic map of the northern Fairbanks mining district, Circle Quadrangle, Alaska: Alaska Division of Geological & Geophysical Surveys Report of Investigation 2011-4, 1 sheet, scale 1:50,000. https://doi.org/10.14509/22642

Streckeisen, A.L., and Le Maitre, R.W., 1979, A Chemical Approximation to the Modal QAPF Classification of the Igneous Rocks: Neues Jahrbuch fur Mineralogie, Abhandlungen, v. 136, p. 169–206.

Twelker, Evan, Werdon, M.B., and Athey, J.E., 2022, Alaska's mineral industry 2020: Alaska Division of Geological & Geophysical Surveys Special Report 76, 75 p. https://doi.org/10.14509/30848

U.S. Geological Survey, 1996, Alaska Resource Data File, (version 1.7, March, 2018): U.S. Geological Survey data release, https://doi.org/10.5066/P96MMRFD

Weber, F.R., McCammon, R.B., Rinehart, C.D., Light, T.D., and Wheeler, K.L., 1988, Geology and mineral resources of the White Mountains National Recreation Area, east-central Alaska: U.S. Geological Survey Open-File Report 88-284, 234 p., 31 sheets, scale 1:63,360. https://dggs.alaska.gov/pubs/id/11727

Weber, F.R., Wheeler, K.L., Rinehart, C.D., Chapman, R.M., and Blodgett, R.B., 1992, Geologic map of the Livengood Quadrangle, Alaska: U.S. Geological Survey Open-File Report 92-562, 20 p., 1 sheet, scale 1:250,000. https://dggs.alaska.gov/pubs/id/11832

APPENDICES

APPENDIX A. MAJOR- AND MINOR-OXIDE AND TRACE-ELEMENT COMPOSITIONS

Major- and minor-oxide analyses in table A1 were performed by ALS Chemex by lithium borate fusion and X-ray fluorescence spectroscopy (Athey and others, 2008). Trace-element values for Nb, Rb, Sr, Y, and Zr were determined at the University of Alaska Fairbanks by XRF on a pressed pellet. Lower and upper detection limits for the trace-element analyses are 0.01 and 100 ppm, respectively. Weight percent CIPW normative compositions were calculated from all igneous rock analyses using the methodology of Irvine and Baragar (1971). Igneous rock names are interpreted from classifications of igneous rocks: Q'-ANOR diagram after Streckeisen and Le Maitre (1979) and R1-R1 diagram after De La Roche and others (1980).

Table A1. Concentrations of major oxides, minor oxides, and trace elements for samples collected in the study area, as measured by X-ray fluorescence at the University of Alaska Fairbanks. Sample 07LF224B was collected from subrounded cobbles in McManus Creek and the location of its bedrock source material is unknown. The sample has a unique texture and composition for this field area, as well as a high magnetic susceptibility (average 29.6 x 10^{-3} SI, maximum 54.7 x 10^{-3} SI). Note: two samples were rerun for certain elements to check for errors. The duplicate analyses are identified with "#2" after the sample number.

Sample Number	Rock name	SiO_2 (%)	Al_2O_3 (%)	Fe_2O_3 (%)	CaO (%)	MgO (%)	Na_2O (%)	K_2O (%)	TiO_2 (%)	MnO (%)	P_2O_5 (%)	Cr_2O (%)	SrO (%)	BaO (%)	Total	Rb (ppm)	Sr (ppm)	Y (ppm)	Zr (ppm)	Nb (ppm)
07MBW335A	Syenogranite	74.76	12.95	2.15	0.7	0.15	2.23	5.27	0.05	0.03	0.011	<0.01	<0.01	0.01	99.86	562	19	109	149	28
07MBW273A	Syenogranite	76.14	12.73	2.12	0.22	0.1	2.72	4.93	0.05	0.03	0.014	<0.01	<0.01	<0.01	99.9	465	18	64	165	27
07MBW290A	Syenogranite	74.72	13.88	1.58	0.6	0.04	3.61	4.47	<0.01	0.03	0.011	<0.01	<0.01	<0.01	99.84	875	25	165	101	41
07MBW275A	Syenogranite	74.45	14.09	1.42	0.65	0.04	3.71	4.56	<0.01	0.04	0.012	<0.01	0.01	<0.01	99.83	896	42	167	92	42
07JEA299A	Hydrothermally altered granite	61.67	19.39	3.89	1.04	0.88	0.17	6.88	0.35	0.13	0.136	<0.01	0.05	0.32	99.91	241	433	69	304	13
07Z156C	Monzogranite	62.44	17.76	4.57	3.22	0.82	2.4	5.39	0.34	0.12	0.132	<0.01	0.16	0.29	99.85	162	1372	37	299	13
07Z159A	Monzogranite	64.46	16.3	4.02	3.54	1.45	2.7	4.87	0.49	0.07	0.183	<0.01	0.14	0.26	99.75	167	1176	22	222	12
07LF158A	Monzogranite	65.87	15.97	3.76	2.56	1.31	3	4.94	0.43	0.07	0.169	<0.01	0.13	0.26	99.89	166	1053	22	203	12
07MBW393A	Monzogranite	65.7	15.9	3.72	2.99	1.31	2.52	5.27	0.43	0.08	0.166	<0.01	0.12	0.24	99.75	218	1022	21	201	12
07LF159A	Monzogranite	66.03	15.96	3.73	3.09	1.28	2.75	4.93	0.42	0.07	0.164	<0.01	0.13	0.23	99.91	178	1074	21	213	12
07RL037B	Monzogranite	66	15.74	3.73	2.59	1.25	2.62	5.27	0.41	0.07	0.163	<0.01	0.12	0.24	99.99	219	982	22	208	12
07MBW382A	Monzogranite	66.12	15.74	3.68	2.75	1.3	2.55	5.04	0.4	0.07	0.159	<0.01	0.12	0.25	99.83	195	1019	22	211	12
07LF146B	Monzogranite	67.34	15.27	2.51	2.33	0.69	3.25	4.04	0.47	0.03	0.176	<0.01	0.03	0.1	99.76	179	210	16	236	23
07MBW395A	Quartz monzonite	55.72	14.95	8.27	5.25	4.19	1.79	4.47	0.99	0.16	0.574	0.01	0.07	0.28	99.89	176	675	48	227	15
07LF162C	Quartz monzonite/ tonalite	57.62	14.88	7.48	4.12	4.14	1.5	4.79	0.85	0.14	0.458	0.01	0.08	0.33	99.72	188	700	36	212	16
07LF163A	Quartz monzonite	59.79	15.57	5.83	3.11	2.7	2.23	5.35	0.64	0.1	0.321	0.01	0.09	0.33	99.9	178	816	25	237	15
07Z160B	Quartz monzonite	62.01	17.06	4.13	3.2	0.76	2.63	5.78	0.32	0.12	0.123	<0.01	0.14	0.28	99.92	185	1224	37	292	14
07Z161A	Granodiorite/tonalite	58.37	14.66	7.9	4.49	4.4	1.45	4.17	0.96	0.13	0.497	0.01	0.07	0.3	99.94	159	652	40	202	16
07LF015B	Schist	88.21	4.61	2.33	0.29	0.52	1.1	0.65	0.27	0.05	0.035	<0.01	<0.01	0.01	98.53	27	28	8	195	5
07Z235A	Quartzite	82.03	7.28	4.53	0.12	1.34	1.88	0.52	0.26	0.03	0.06	<0.01	0.02	0.04	99.36	22	122	14	188	7
07JEA250A	Schist	65.61	10.75	10.45	2.92	4.37	1.14	0.46	1.33	0.13	0.064	0.02	0.01	0.01	99.84	16.7	60.3	18.2	149.6	5.9
07Z377A	Schist	60.45	15.54	9.85	0.43	3.65	3.38	1.18	1.12	0.1	0.058	0.02	0.01	0.03	99.52	40	101	18	155	8

Table A1, continued. Concentrations of major oxides, minor oxides, and trace elements for samples collected in the study area, as measured by X-ray fluorescence at the University of Alaska Fairbanks.

Sample Number	Rock name	SiO_2 (%)	Al_2O_3 (%)	Fe_2O_3 (%)	CaO (%)	MgO (%)	Na_2O (%)	K_2O (%)	TiO_2 (%)	MnO (%)	P_2O_5 (%)	Cr_2O (%)	SrO (%)	BaO (%)	Total	Rb (ppm)	Sr (ppm)	Y (ppm)	Zr (ppm)	Nb (ppm)
07Z035A	Schist	57.04	16.46	11.22	0.85	4.11	2.52	2.37	1.21	0.12	0.111	0.02	0.02	0.05	99.88	73	163	24	150	9
07Z035A, #2	Schist	---	---	---	---	---	---	---	---	---	---	---	---	---	---	74	163	24	152	9
07MBW326A	Schist	55.98	17.5	11.34	1.85	3.5	1.53	2.97	1.23	0.11	0.101	0.02	0.01	0.03	99.71	106	47	30	165	10
07MBW029A	Schist	51.07	23.56	10.33	0.42	2.89	0.56	5.13	1.1	0.18	0.13	0.01	0.02	0.11	99.69	171	142	38	141	23
07MBW025B	Schist	42.73	15.5	17.92	1	12.71	0.06	0.01	1.15	0.23	0.221	0.1	<0.01	<0.01	99.84	2	24	8	94	24
07LF224B	Amphibolite, within-plate	42.44	9.04	15.31	12.21	12.61	1.13	0.35	2.56	0.24	0.763	0.11	0.03	0.02	99.7	1	261	21	102	17
07LF224B, #2	Amphibolite, within-plate	---	---	---	---	---	---	---	2.56	---	---	---	---	---	---	2	274	22	108	18
07Z087A	Mafic semischist, within-plate	41.14	13.68	11.92	8.3	9.79	3.02	0.42	3.24	0.19	0.663	0.05	0.05	0.01	99.85	34	447	29	229	59
07Z036A	Amphibolite, within-plate	45	18.25	11.6	10.34	4.55	3.27	0.38	3.13	0.14	0.319	0.02	0.11	0.07	99.93	5	1046.2	14	167.4	31.7
07LF056A	Mafic schist, within-plate	42.73	17	15.16	3.67	6.45	2.03	1.15	4.3	0.22	0.808	0.02	0.02	0.04	99.82	42	149	34	394	87
07MBW487A	Mafic schist, arc	45.01	14.04	16.31	6.82	6.93	0.11	0.94	2.11	0.22	0.111	0.03	0.01	0.02	99.76	34	73	34	275	11
07MBW646A	Mafic schist, arc	50.92	11.7	15.69	8.23	7.4	1.31	0.2	2.32	0.22	0.069	0.04	0.01	0.01	99.94	4	77	21	122	7
07MBW320A	Mafic schist, arc	48.68	14.15	14.54	8.75	6.96	1.47	0.2	1.89	0.2	0.075	0.03	0.01	<0.01	99.85	8	112	22	100	6
07LF221B	Mafic schist, arc	50	13.98	11.58	8.48	5.84	0.92	0.42	1.43	0.14	0.075	0.03	0.02	0.01	99.99	13	134	19	93	5
07JEA249A	Mafic schist, arc	49.72	15.96	14.81	6.44	5.85	1.77	0.52	2.04	0.17	0.107	0.03	0.01	0.01	99.8	16.9	104.9	26.8	149.8	7.9
07LF222A	Mafic semischist, arc	53.66	15.46	11.18	8.56	4.75	1.79	0.31	1.14	0.14	0.077	0.02	0.02	<0.01	99.84	10	139	19	86	5
07LF070A	Mafic schist, arc	53.01	16	12.03	6.89	5.09	2.68	0.32	1.29	0.16	0.09	0.02	0.02	0.01	99.81	8	200	22	97	5
07MBW367A	Mafic schist, arc	52.27	15.38	14.04	5	6.22	1.05	0.23	1.56	0.18	0.094	0.03	0.01	0.01	99.87	12	102	26	124	7
07Z255A	Mafic semischist, arc	50.69	16.7	13.09	7.57	5.48	2.28	0.24	1.36	0.17	0.117	0.02	0.02	0.01	99.87	11	145	24	107	6
07MBW627A	Mafic schist, arc	48.97	16.8	11.67	10.05	4.87	0.51	0.37	1.22	0.16	0.078	0.02	0.02	0.01	99.86	17	194	21	115	6
07Z215A	Mafic schist, arc	48.49	16.14	13.43	6.55	5.49	1.47	0.8	1.65	0.2	0.138	0.02	0.01	0.01	99.77	39	129	38	195	11
07MBW365A	Mafic schist, arc	53.55	16.96	13.16	3.04	4.61	2.87	0.96	1.39	0.14	0.165	0.02	0.02	0.02	99.83	39	178	36	166	10
07JEA173A	Mafic schist, arc	50.6	18	13.96	3.52	5.1	2.46	1.54	1.61	0.14	0.14	0.02	0.01	0.03	99.7	50.3	103.1	40.9	213.7	14.4
07Z040A	Amphibolite, arc	48.65	19.96	11.46	2.91	5.15	2.55	2.57	1.31	0.16	0.271	0.02	0.01	0.08	99.92	65	115	38	173	12

APPENDIX B. TRACE-ELEMENT-INDICATED TECTONIC SETTINGS OF IGNEOUS AND METAMAFIC ROCKS

Tectonic setting for igneous and metamafic rocks from the study area as indicated by trace-element discrimination diagrams.

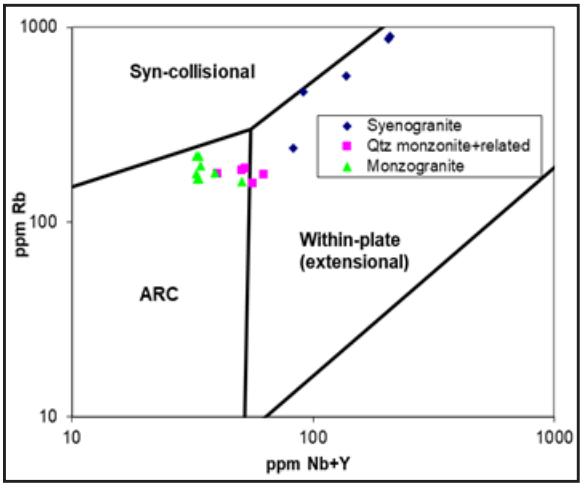

Figure B1. Felsic igneous rocks plotted on Rb vs. Nb + Y discrimination diagram for rhyolites. Diagram after Pearce and others (1984).

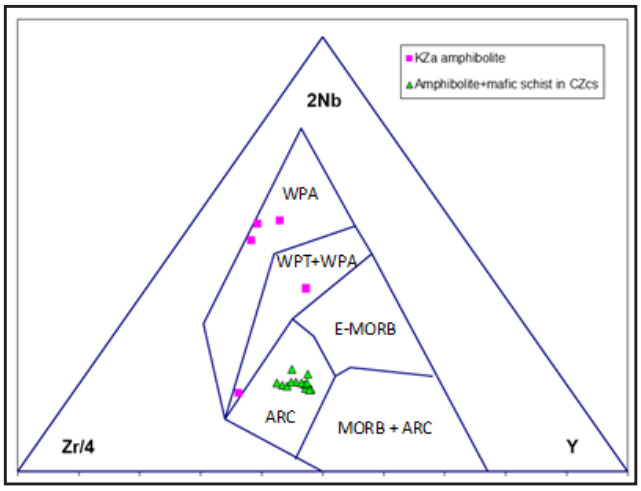

Figure B2. Mafic metaigneous rocks and metagraywacke plotted on the Nb-Zr-Y discrimination diagram for basalts. Diagram after Meschede (1986). Note: WPA = within-plate alkalic, WPT = within-plate tholeiitic, MORB = mid-ocean ridge basalt, E-MORB = extensional, mid-ocean ridge basalt, and ARC = island arc/subduction-related.

APPENDIX C. NON-CARBONATE-CARBON ANALYSES

Table C1. Analysis of 16 samples for non-carbonate-carbon content.

Sample Number	Organic carbon (percent)
07JEA063A	0.06
07JEA064A	0.21
07JEA212A	0.38
07JEA353A	<0.01
07LF181A	0.15
07LF203A	0.19
07LF227A	0.07
07MBW696A	0.39
07RN138C	0.28
07RN139A	0.72
07RN140A	0.94
07RN141A	1.16
07RN146A	0.85
07RN157AC	0.21
07RN163B	0.13
07Z413A	15.10

Organic carbon analyses were performed by ALS Chemex (table C1). Rock samples were crushed with a Terminator oscillating jaw crusher with chrome steel alloy plates so that at least 70 percent of the material passed through a -10 mesh (2 mm) screen. Representative aliquots of 250 grams each were taken using a stainless-steel riffle splitter. These samples were then pulverized in an Essa ring mill bowl and pucks made of Essa's Standard Steel alloy so that 85 percent of the sample passed through a -200 mesh (75 micron) screen. Non-carbonate-carbon content was determined using a LECO furnace after a dilute acid digestion (C-IR06). Lower and upper detection limits are 0.01 percent and 50 percent, respectively. Analysis of sample 07RN157AC is for combined samples 07RN157A and 07RN157C.

APPENDIX D. ELECTRON MICROPROBE ANALYTICAL RESULTS

Samples were analyzed using the Cameca SX-50 electron microprobe at the Advanced Instrumentation Laboratory at the University of Alaska Fairbanks. Garnet–biotite geothermometry and garnet–plagioclase–muscovite–biotite equilibria geobarometry were conducted on 16 samples to assess the metamorphic history of the units. See table D1 for the geothermometers and geobarometers employed. Garnet–biotite thermometers were selected for use based on their appropriateness for manganese, calcium, and other elements in samples. The approximate intersection of plotted data from the listed garnet–plagioclase–muscovite–biotite geobarometers was used to estimate the pressure. Error was estimated based on an ellipse tilted slightly to higher pressures and temperatures, and uncertainty is reported as a plus or minus value (±) for each pressure or temperature estimate. Compositional information was collected on other metamorphic minerals to provide additional insight into the area's metamorphic history.

Table D1. References used in geothermometer and geobarometer calculations.

Primary garnet–biotite thermometry models and resources employed:

Kleeman, Ulrich, and Reinhardt, Juergen, 1994, Garnet–biotite thermometry revisited: The effect of AlVI and Ti in biotite: European Journal of Mineralogy, v. 6, p. 925–941.

Berman, R.G., 1990, Mixing properties of Ca–Mg–Fe–Mn garnets: American Mineralogist, v. 75, p. 328–334. (garnet model)

Secondary garnet–biotite thermometry models and resources employed:

Perchuk, L.L., and Lavrenteva, I.V., 1984, Experimental investigation of exchange equilibria in the system cordierite-garnet-biotite, *in* Saxena, S.K., ed., Kinetics and Equilibrium in Mineral Reactions: Springer Verlag, New York, p. 199–240.

Ganguly, Jibamitra, and Saxena, S.K., 1984, Mixing properties of aluminosilicate garnets: Constraints from natural and experimental data, and applications to geothermobarometry: American Mineralogist, v. 69, p. 88–97. (garnet model)

Hodges, K.V., and Spear, F.S., 1982, Geothermometry, geobarometry and the Al2SiO5 triple point at Mt. Moosilauke, New Hampshire: American Mineralogist, v. 67, p. 1118–1134.

Patino-Douce, A.E., Johnston, A.D., and Rice, J.M., 1993, Octahedral excess mixing properties in biotite: A working model with applications to geobarometry and geothermometry: American Mineralogist, v. 78, p. 113–131.

Garnet–plagioclase–muscovite–biotite equilibria geobarometers employed:

Ghent, E.D., and Stout, M.Z., 1981, Geobarometry and geothermometry of plagioclase-biotite-garnet-muscovite assemblages: Contributions to Mineralogy and Petrology, v. 76, p. 92–97.

Hodges, K.V., and Crowley, P.D., 1985, Error estimation and empirical geothermobarometry for pelitic systems: American Mineralogist, v. 70, p. 702–709.

Powell, Roger, and Holland, T.J.B., 1988, An internally consistent thermodynamic dataset with uncertainties and correlations: 3. Applications to geobarometry, worked examples and a computer program: Journal of Metamorphic Geology, v. 6, p. 173–204.

Hoisch, T.D., 1990, Empirical calibration of six geobarometers for the mineral assemblage quartz + muscovite + biotite + plagioclase + garnet: Contributions to Mineralogy and Petrology, v. 104, p. 225–234.

Each is employed using either the Berman, R.G. (1990) or Ganguly, Jibamitra, and Saxena, S.K. (1984) garnet model.

Aluminosilicate phase diagram:

Holdaway, M.J., 1971, Stability of andalusite and the aluminum silicate phase diagram: American Journal of Science, v. 271, p. 97–131.

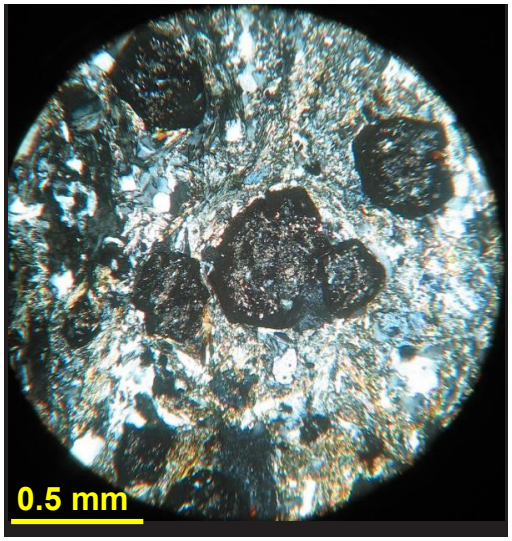

Figure D1. Isotropic garnet in sample 07JEA249A showing zoned, prograde metamorphism. Photo from microscope with cross-polarized light and 10x magnification.

The metapelitic prograde mineral assemblage is garnet, quartz, plagioclase porphyroblasts, muscovite/phengite, paragonite, biotite, and chlorite. Retrograde greenschist minerals in the metapelites include albite, chloritoid, and chlorite. Garnet and plagioclase porphyroblasts are syn-tectonic; foliation is preserved in the rotated crystals. Garnets appear pink in hand sample because of numerous quartz inclusions; garnet porphyroblasts typically contain about 50 percent garnet and 50 percent quartz. The garnets characteristically display retrograded cores and clear rims. Compositional data confirm a prograde metamorphic trend, either as a relatively smooth transition from lower to higher pressure–temperature (P–T) conditions (fig. D1) or as two cycles of increasing metamorphic grade (fig. D2). The atomic Fe/Mg ratio displayed in figure D2 shows this most effectively. Garnet compositions from the study area are similar to Fairbanks amphibolite-facies garnets, with a lower pyrope (Mg) component than those recorded for Fairbanks eclogite facies rocks (this study; Brown and Forbes, 1986; Newberry, R.J, unpublished data, 2006).

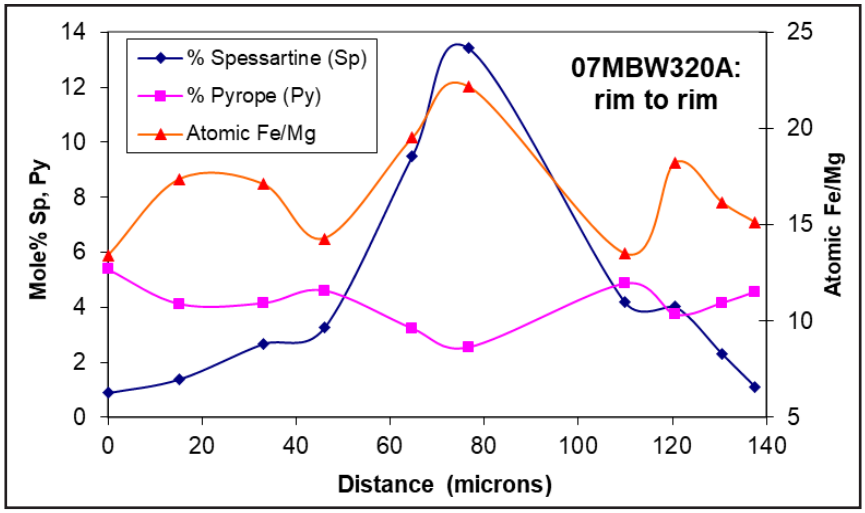

Figure D2. Microprobe traverse across a garnet from schist sample 07MBW320A showing two cycles of prograde metamorphism.

Prograde metamorphism is also apparent in some amphiboles from metamafic rocks (unit KZa and amphibolite and mafic schist from unit ЄZcs), which have actinolite cores with hornblende rims (fig. D3). Both the within-plate and arc-related metamafic rocks show their highest P–T condition as epidote–amphibolite facies. Some metamafic samples only contain the greenschist assemblage actinolite–clinozoisite–calcite–quartz; the samples may be completely retrograded after amphibolite facies or a prograde assemblage that never made it to amphibolite grade. Alternatively, the greenschist-facies samples may not have been subjected to amphibolite-facies pressures and temperatures long enough to recrystallize the rock. Fairbanks area metabasalt to the west is completely recrystallized to epidote–amphibolite facies and then retrograded to greenschist facies (Newberry and others, 1996).

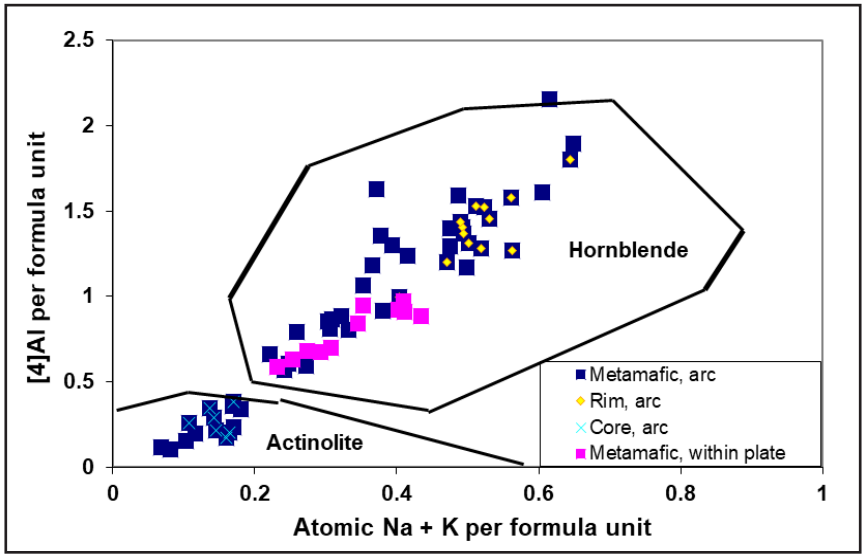

Figure D3. Amphibole compositions from metamafic rocks in the study area. Fields after Deer and others, 1997.

Study area P–T conditions are similar to those in the Fairbanks area but show a wider spread of higher pressures and temperatures through upper greenschist and epidote–amphibolite facies (table D2; fig. D4). The resulting pressures in particular show a large spread from 5.5 to 9 kbar, perhaps reflecting exhumation at different levels and structural complexity.

Table D2. Results from garnet–biotite geothermometry and garnet–plagioclase–muscovite–biotite equilibria geobarometry. Pressure estimates were not obtained from two samples lacking plagioclase.

Number	Sample ID	Sample description	Pressure (kbar)	Temperature (°C)
1	07JEA102A	chlorite–calcite–garnet–biotite–white mica–feldspar–quartz schist	7±1	475±20
2	07JEA172A	biotite–garnet–white mica–feldspar–quartz schist	8±1	550±25
3	07JEA311A	chloritoid–biotite–white mica–garnet–feldspar–quartz schist	8.5±1	580±20
4	07MBW038A	garnet–biotite–chlorite–while mica–feldspar–quartz semischist	5.5±1	460±20
5	07MBW088A	chlorite–white mica–biotite–garnet–feldspar–quartz schist	6.5±1	480±20
6	07MBW102A	garnet–biotite–white mica–feldspar–quartz schist	8±1	510±20
7	07MBW320A	garnet–biotite –chlorite–white mica–quartz schist	N/A	500±30
8	07MBW367A	biotite–garnet–chlorite–white mica–feldspar–quartz schist	8.5±1	600±20
9	07MBW527A	calcite–chlorite–biotite–white mica–garnet–quartz–plagioclase semischist	7±1	485±15
10	07MBW646A	garnet–chlorite–biotite–quartz schist	N/A	485±20
11	07RL017A	garnet–biotite–feldspar–white mica quartzite	8±1	535±20
12	07RL062A	garnet–biotite–white mica–feldspar–quartz schist	9±1	600±20
13	07RN062A	garnet–chlorite–white mica–biotite–feldspar–quartz schist	7±1	480±20
14	07Z017B	garnet–biotite–feldspar–white mica quartzite	9±1	540±20
15	07Z417A	hornblende–quartz–garnet–white mica–biotite–feldspar semischist	9±1	550±20
16	07Z446B	biotite–white mica–garnet–feldspar quartzite	7±1	460±20

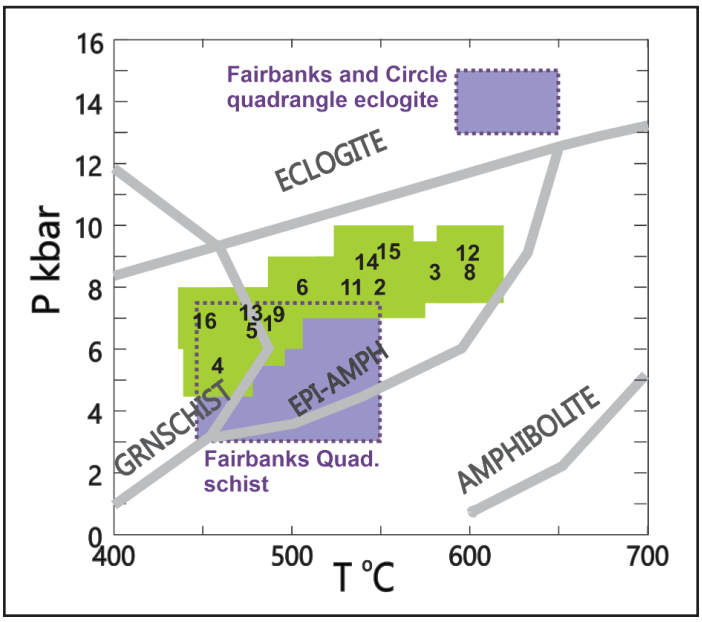

Figure D4. Pressure–temperature conditions of study area (green; this study) compared with Fairbanks area (purple; Brown and Forbes, 1986; Joy and others, 1996; Newberry and others, 1996; Douglas and others, 2002). Sample data are referenced from table D2; the number of the sample is the approximate centroid of the error rectangle.

APPENDIX E. $^{40}AR/^{39}AR$ ANALYSES

Five samples were submitted to the University of Alaska Fairbanks Geochronology Laboratory for $^{40}Ar/^{39}Ar$ analysis. The samples were crushed, washed, and sieved to either 100–250- or 250–500-micron size fractions, and handpicked for datable mineral phases. For sample 07Z417A, both biotite and hornblende were analyzed. Analyses were conducted according to the procedures outlines in Benowitz and others, 2011.

A summary of results is given in table E1, with all ages quoted to the ±1 sigma level and calculated using the constants of Steiger and Jaeger (1977; Layer and others, in prep.). The integrated age is the age given by the total gas measured and is equivalent to a potassium-argon (K-Ar) age. The spectrum provides a plateau age if three or more consecutive gas fractions represent at least 50 percent of the total gas release and are within two standard deviations of each other (Mean Square Weighted Deviation [MSWD] less than ~2.7). All samples showed well-defined plateaus except hornblende from 07Z417A, which presented "plateau-like" fractions (a pseudo-plateau) but did not meet the criteria for a true plateau.

Table E1. $^{40}Ar/^{39}Ar$ interpretive details. Bold text indicates preferred ages for each sample (ages reported at ±1 sigma).

Number	Sample	Mineral	Integrated Age (Ma)	Plateau Age (Ma)	Plateau Information	Other Comments
A1	07MBW335A	biotite	57.3 ± 0.2	56.8 ± 0.2	9 fractions 66% 39Ar release MSWD = 2.1	Syenogranite; slight amount of excess argon
A2	07JEA299A	sericite	72.4 ± 0.4	72.1 ± 0.4	11 fractions 93% 39Ar release MSWD = 0.8	Hydrothermally altered granite; last step (1.5% release) steps up to 86 Ma. Resetting?
A3	07Z161A	biotite	90.9 ± 0.3	91.2 ± 0.3	9 fractions 93% 39Ar release MSWD = 1.2	Granodiorite; first step (0.7% release) has an age of 60 Ma
A4	07Z159A	hornblende	93.6 ± 0.5	92.5 ± 0.5	5 fractions 96% 39Ar release MSWD = 1.4	Granodiorite; isochron age identical to plateau age
A5	07Z417A	biotite	95.7 ± 0.4	101.7 ± 0.6	11 fractions 60% 39Ar release MSWD = 2.1	Semischist; argon loss models to 5% loss at ~15 Ma
A6	07Z417A	hornblende	145.4 ± 0.8	144 ± 4	7 fractions 75% 39Ar release MSWD = 26	Semischist; pseudo-plateau. Age reflects average of "plateau-like" fractions

APPENDIX F. DETRITAL ZIRCON ANALYSIS

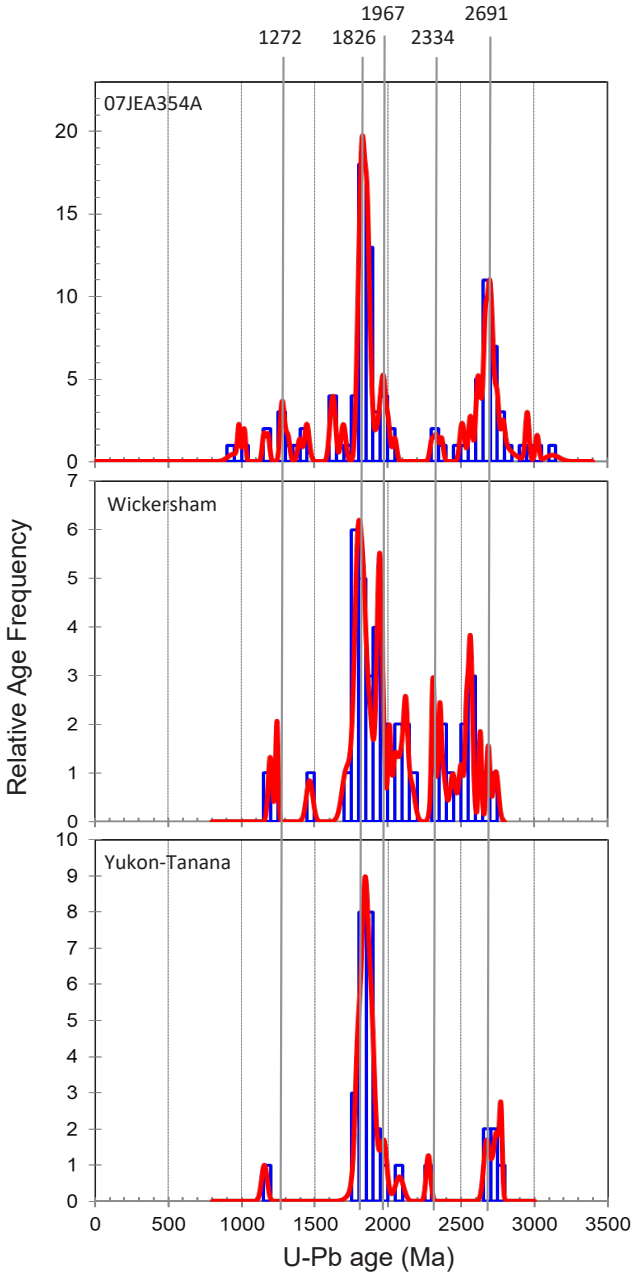

Figure F1. Comparison of probability–density plots among detrital zircon data from sample 07JEA354A, a metasandstone from unit ЄZq on Mt. Ryan with up to 70 percent 1-mm "grit" grains of quartz + feldspar (O'Sullivan and Athey, in prep.), and grit-bearing rocks from the Wickersham and Yukon-Tanana terranes (Bradley and others, 2007). The analyses for each sample were plotted using Isoplot v. 4.15.

Detrital zircons were analyzed from sample 07JEA354A (O'Sullivan and Athey, in prep.). Zircons were separated at the Apatite-to-Zircon, Inc. laboratory using heavy liquid and magnetic separation techniques. Grains were mounted in epoxy and polished to expose grain interiors for analysis. One-hundred-five grains were selected at random and dated from the sample. Uranium, thorium, and lead isotope data were collected at the Washington State University Geoanalytical Laboratory on a ThermoFinnigan Element2 magnetic sector double-focusing ICP–MS (inductively coupled plasma–mass spectrometer). Each grain underwent laser ablation using a New Wave Research UP-213 system. See Chang and others (2006) for additional details regarding laboratory procedures such as standards and error corrections.

Of the 105 grains analyzed from sample 07JEA354A, five analyses were rejected. Preferred ages for 93 grains were generally taken from the $^{206}Pb/^{238}U$ age if less than 1500 Ma or from the $^{207}Pb/^{206}Pb$ age if greater than 1500 Ma. For seven grains with undefined ages, the intercept age of the discordia with the concordia with the lowest relative error (either the upper- or lower-intercept age) was used. The age distribution data for the sample are plotted in histogram format and cumulative probability curves (fig. F1). Histograms illustrate the number of ages that fall into each 50 Ma bin. Cumulative probability curves, which are a common method for displaying detrital zircon data, represent the normalized sum of probability distributions for all analyses from a sample. Age peaks are only considered statistically significant if defined by several analyses.